
MeGA: Hybrid Mesh-Gaussian Head Avatar for High-Fidelity Rendering and Head Editing

Cong Wang^{1,2}, Di Kang², He-Yi Sun¹, Shen-Han Qian³, Zi-Xuan Wang⁴,
Linchao Bao⁵, Song-Hai Zhang¹

¹Tsinghua University, ²Tencent AI Lab, ³Technical University of Munich,
⁴Carnegie Mellon University, ⁵University of Birmingham

Abstract

Creating high-fidelity head avatars from multi-view videos is a core issue for many AR/VR applications. However, existing methods usually struggle to obtain high-quality renderings for all different head components simultaneously since they use one single representation to model components with drastically different characteristics (e.g., skin vs. hair). In this paper, we propose a Hybrid **Mesh-Gaussian Head Avatar** (MeGA) that models different head components with more suitable representations. Specifically, we select an enhanced FLAME mesh as our facial representation and predict a UV displacement map to provide per-vertex offsets for improved personalized geometric details. To achieve photorealistic renderings, we obtain facial colors using deferred neural rendering and disentangle neural textures into three meaningful parts. For hair modeling, we first build a static canonical hair using 3D Gaussian Splatting. A rigid transformation and an MLP-based deformation field are further applied to handle complex dynamic expressions. Combined with our occlusion-aware blending, MeGA generates higher-fidelity renderings for the whole head and naturally supports more downstream tasks. Experiments on the NeRSemble dataset demonstrate the effectiveness of our designs, outperforming previous state-of-the-art methods and supporting various editing functionalities, including hairstyle alteration and texture editing.

1 Introduction

Achieving photorealistic rendering of animatable head avatars has consistently been a focal topic in computer vision and computer graphics, with extensive applications in fields such as AR/VR communications [10, 24, 19], gaming [31], and remote collaborations[34].

Existing methods have explored mesh-based representations [19, 23, 9, 1], NeRF-based representations [37, 32, 12, 22], and 3D Gaussians-based representations [26, 6, 36, 33] and achieved remarkable progress in this field. However, the human head is a complex “object” containing components with drastically different characteristics (e.g., skin vs. hair) so there may not exist one single representation that can model all of them well simultaneously. For instance, the human hair contains volumetric thin structures while the human face is predominantly flat regions and can be animated in a low dimensional space [18]. Thus, using one single representation to model all different head components inevitably sacrifices the rendering quality of one part for another.

Ideally, we expect the head avatar representation can be rendered in photorealistic quality and can be easily controlled to perform vivid facial animations. For high-quality *facial* rendering, Pixel Codec Avatars (PiCA) [23], which adopts neural texture representation [30], have demonstrated extraordinary rendering quality and subtle dynamic texture details while being highly efficient due to its adoption of rasterization and deferred neural rendering. However, it contains noticeable artifacts

including texture-like hair rendering and mesh-like hair boundaries. In contrast, GaussianAvatars [26], which adopts rigged 3D Gaussian Splatting (3DGS) [15] representation, successfully reconstructs high-frequency volumetric human hair but shows inferior facial texture details (e.g., wrinkles). In addition, another advantage that comes with using mesh-based representation for face modeling is that it greatly eases facial appearance editing and animation.

Therefore, we propose to use more suitable representations for different head components (i.e., neural mesh for the face and 3DGS for the hair), resulting in a Hybrid **M**esh-**G**aussian Head **A**vatar (MeGA). Specifically, we adopt the FLAME mesh model [18] as our base mesh to model dynamic human faces. Additionally, we learn a UV displacement map conditioned on the driving signal (i.e., FLAME parameters) to account for the geometric details that cannot be represented in the FLAME space. To achieve photorealistic rendering, we use neural texture and deferred neural rendering [30, 23]. Different from [23], our neural texture consists of three components, including a diffusion texture map to model the base color, an *expression-dependent* texture map to model dynamic textures (e.g., forehead wrinkles and dimples), and a *view-dependent* texture map to handle view-dependent effects. For hair modeling, a static 3DGS representation is first built for a chosen canonical frame and then deformed using an MLP network to capture the hair dynamics.

Another crucial component of MeGA is properly blending the face and hair images. Due to the existence of the head mesh, we need to correctly exclude the contributions from the Gaussians occluded by the mesh. To this end, we propose an early-stopping strategy for the Gaussian hair rendering, resulting in an occlusion-aware blending module.

Due to the decomposed representation, MeGA not only produces high-quality rendering results for the whole head but also enables various downstream operations, including hairstyle alterations and texture editing.

In summary, our contributions include:

- We are the first to propose a hybrid mesh-Gaussian full-head representation, adopting more suitable representations to model different head components (i.e., neural mesh for the face, 3DGS for the hair).
- The decomposed hybrid representation naturally supports various downstream applications, including high-quality hair alteration and texture editing.
- Experimental results on the NeRSemble dataset demonstrate that our approach produces higher-quality renderings for novel view synthesis and novel expression synthesis.

2 Related Works

2.1 Animatable Head Avatars

Creating high-fidelity, animatable 3D head avatars from images or videos has always been of great interest in the computer vision and graphics community. Traditional explicit geometric modeling methods [14, 13, 2] usually rely on low-poly meshes and suffer from inaccurate details, especially around hair regions. With the rise of neural network-based approaches, Codec Avatars [19, 23, 21, 35, 32] utilize coarse tracked meshes together with neural networks to model and render facial performance sequences by capturing them from multi-view videos. The captured avatars can be animated using a driving model [19] that translates control signals into the avatar latent codes; however, this approach may lack intuitive controls. Another line of work [7, 9, 11, 41, 8, 42, 38, 40, 44, 26, 36] aims to model head avatars that can be directly driven using parameters from existing parametric face models (e.g., FLAME [18]). It is noteworthy that methods utilizing multi-view video inputs [26, 36] typically significantly outperform those relying on monocular inputs [7, 9, 11, 41, 8, 42, 38, 40, 44]. Our work follows the multi-view video setting like the GaussianAvatars [26].

2.2 3D Representations for Head Avatars

Traditional 3D head avatars [14, 13, 2] typically employ a topological consistent, morphable mesh model (3DMM) [4, 18] for face modeling and animation. However, it is exceedingly challenging to faithfully reconstruct the intricate details of the face and complicated hair regions using standard 3DMMs. To address these challenges, implicit head avatar models integrate neural networks into the avatar modeling and rendering processes. For instance, the Neural Head Avatar [9] and IM

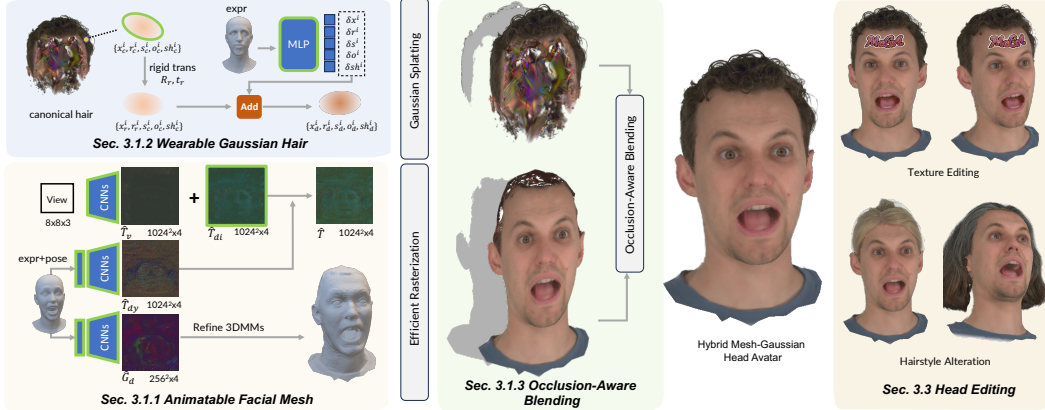


Figure 1: **Overview of our Hybrid Mesh-Gaussian Head Avatar.** MeGA models different head components with more suitable representations. For *facial* modeling, we propose a neural mesh-based representation, including a UV displacement map \hat{G}_d for geometric details, a disentangled neural texture map composed by \hat{T}_{di} , \hat{T}_{dy} , and \hat{T}_v to learn the diffuse colors, dynamic textures, and view-dependent colors, respectively. For *hair* modeling, a canonical 3D Gaussian Splatting is reconstructed and then animated using a global rigid transformation and an MLP-based non-rigid deformation field. A mesh occlusion-aware blending is proposed to properly blend the face and hair images. MeGA naturally supports hair alteration and texture editing due to the disentangled representations. Learnable parameters are highlighted using green boxes.

Avatar [41] leverage neural networks to model the geometric and texture details beyond the FLAME model [18]. The Deferred Neural Rendering [30] approach achieves high-quality, photorealistic rendering with imperfect 3D assets by substituting the graphics rendering pipeline with a neural network-based rendering process. In addition to the mesh-based representations, there are research works based on point-based representations [42, 32], volume-based representations [20, 38], the mixture of volumetric primitives [21], NeRF-based representations [7, 11, 8, 40], and more recent 3D Gaussians-based representations [26, 36, 6, 33]. Different from previous methods, we employ a hybrid mesh-Gaussian representation to decouple the modeling of human faces and hair. Note that GaussianAvatars [26] also includes a mesh to guide the deformation of 3DGS. However, their mesh is not involved in the rendering process, and thus cannot utilize neural dynamic textures to better model the skin details (e.g., wrinkles).

3 Hybrid Mesh-Gaussian Head Avatar

The input to our method is a set of multi-view videos of a subject. We aim to create an animatable head avatar for the subject, which can be driven by FLAME parameters. Specifically, as shown in Fig. 1, given the driving signal (e.g., FLAME shape β , expression ψ , and pose ϕ parameters) for modeling facial mesh, we employ three decoders to generate a UV displacement map \hat{G}_d , a view texture map \hat{T}_v , and a dynamic texture map \hat{T}_{dy} . The UV displacement map \hat{G}_d is used to account for the geometric details that cannot be represented in the FLAME space. The view texture map \hat{T}_v , dynamic texture map \hat{T}_{dy} and diffuse texture map \hat{T}_{di} are added up to generate facial neural textures \hat{T} . Facial colors are then obtained using efficient mesh rasterization followed by a per-pixel decoder. For hair modeling, we create a static canonical 3DGS and further introduce a rigid global transformation and an MLP-based non-rigid deformation field for animation. Finally, a mesh occlusion-aware blending is proposed to properly blend the face and hair images.

3.1 Animatable Facial Mesh

To achieve accurate control of head avatars and good generalization to unseen expressions, we employ an enhanced FLAME mesh as our facial representation and predict a UV displacement map for

personalized geometric details. Disentangled neural textures are mapped to this refined facial mesh and decoded into RGB colors using our per-pixel texture decoder.

Enhanced FLAME Mesh. To enhance the expressiveness of FLAME mesh, similar to [9], we densify the FLAME mesh using four-way subdivision and add faces for human teeth, generating our enhanced FLAME mesh:

$$\mathcal{T}(\beta, \psi, \phi) = \{\mathcal{V}(\beta, \psi, \phi), \mathcal{F} \mid \mathcal{V} \in \mathbb{R}^{16428 \times 3}, \mathcal{F} \in \mathbb{R}^{40212 \times 3}\}, \quad (1)$$

where \mathcal{V} describes the vertices of our enhanced mesh which are calculated using the shape $\beta \in \mathbb{R}^{300}$, the expression $\psi \in \mathbb{R}^{100}$, and pose $\phi \in \mathbb{R}^{15}$ parameters based on linear blend skinning (LBS). \mathcal{F} shows the faces of the enhanced mesh.

Geometry Refinement. Based on the enhanced FLAME mesh, inspired by [32, 29], we predict a UV displacement map \hat{G}_d conditioned on FLAME expression parameters ψ and pose parameters ϕ , and our refined mesh \mathcal{T}_r is obtained by:

$$\begin{aligned} \mathcal{T}_r(\beta, \psi, \phi) = \{ & \mathcal{V}_r(\beta, \psi, \phi), \mathcal{F} \mid \mathcal{V}_r \in \mathbb{R}^{16428 \times 3}, \mathcal{F} \in \mathbb{R}^{40212 \times 3}\}, \\ & \text{where } \mathcal{V}_r(\beta, \psi, \phi) = \mathcal{V}(\beta, \psi, \phi) + \mathcal{S}(\hat{G}_d), \end{aligned} \quad (2)$$

Here, $\mathcal{S}(\cdot)$ refers to sample values according to UV coordinates of vertices.

Compared to previous geometry refinement networks [9] which use MLPs to predict per-vertex offsets, our UV displacement map naturally ensures the smoothness of the refined mesh due to the locality of Convolutional Neural Networks (CNNs). Further due to the use of $\mathcal{S}(\cdot)$, our geometry refinement supports unlimited mesh resolution, i.e., the computation cost does not increase as the number of vertices increases.

Disentangled Neural Texture. Given the advantages of neural textures to express high-quality dynamic textures and render efficiently, we employ deferred neural rendering [30] to generate colors for facial regions. To model observations more reasonably for better renderings, we disentangle neural textures $\hat{T} \in \mathbb{R}^{1024 \times 1024 \times 4}$ into three parts:

$$\hat{T} = \hat{T}_{di} + \hat{T}_v + \hat{T}_{dy}, \text{ where } \hat{T}_{di}, \hat{T}_v, \hat{T}_{dy} \in \mathbb{R}^{1024 \times 1024 \times 4}. \quad (3)$$

The diffuse texture \hat{T}_{di} is modeled as learnable parameters and used to show the diffuse colors of each face. The view texture \hat{T}_v and dynamic texture \hat{T}_{dy} are predicted using CNNs conditioned on view vectors d and FLAME expression parameters ψ respectively to handle view-dependent effects and dynamic textures (e.g., wrinkles and dimples).

Per-Pixel Texture Decoding. For fast and high-fidelity rendering, we employ per-pixel decoding [23] to obtain RGB colors. Different from [23], to ensure better generalization performance on unseen expressions, our RGB colors are only regressed from UV coordinates and neural textures. Removal of the XYZ coordinate inputs prevents the per-pixel decoder from overfitting to a specific coordinate system, thereby improving the renderings for unseen expressions.

3.2 Wearable Gaussian Hair

We adopt 3DGS [15] for hair modeling since it can better reconstruct high-frequency volumetric objects than mesh-based representations [23, 9]. Specifically, we first choose one training frame (all views) to build a 3DGS-based canonical human hair for static modeling. During the dynamic modeling of the hair, we first compute a rigid transformation using the ICP algorithm [3] to align the canonical hair to a new frame and learn a deformation field (represented as a lightweight MLP) [5, 27, 43] to handle the slight non-rigid movement.

Preliminaries: 3D Gaussian Splatting. Given calibrated multi-view images and an initial point cloud (e.g., from SfM [28]), a *static* scene can be reconstructed using a set of anisotropic Gaussians $\mathcal{G} = \{x^i, r^i, s^i, o^i, sh^i\}_{i=1:N}$, where i represents i -th Gaussian, N the number of Gaussians, $x^i \in \mathbb{R}^3$ the center of the i -th Gaussian, $r^i \in \mathbb{R}^4$ the orientation (represented using a unit quaternion), $s^i \in \mathbb{R}^3$ the scale, $o^i \in \mathbb{R}$ the opacity, and $sh^i \in \mathbb{R}^{48}$ the spherical harmonics coefficients (up to degree 3) used to model view-dependent appearance.

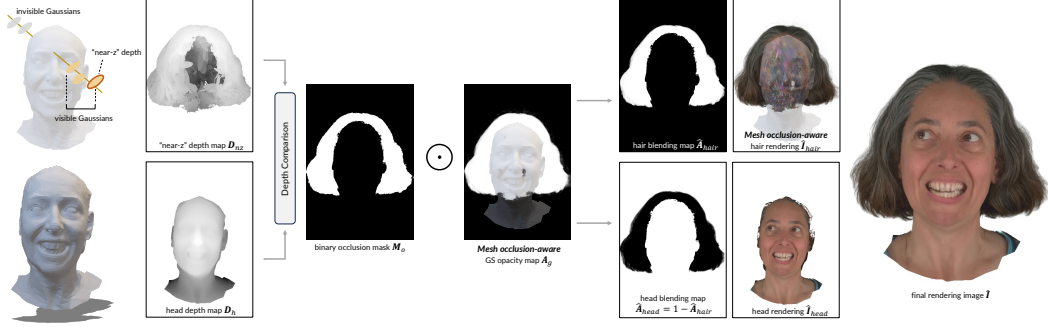


Figure 2: **Mesh Occlusion-Aware Blending.** By comparing the “near-z” depth map $D_{n,z}$ of hair and the depth map of the head, we find pixels that should use hair renderings (white regions in M_o). Further combining with *mesh occlusion-aware* hair opacity map A_g which only accumulates opacities of visible Gaussians (i.e., in front of the mesh), we obtain the blending mask for final renderings.

When rendering a pixel’s color C , all 3d Gaussians intersected with its view vector \mathbf{d} are blended using alpha blending:

$$C = \sum_{i=1} c_i \alpha'_i \prod_{j=1}^{i-1} (1 - \alpha'_j), \quad (4)$$

where c_i is the color of i -th Gaussian computed from sh^i and \mathbf{d} . The blending weight α'_i is given by evaluating the 2D projection of the i -th Gaussian multiplied by o^i . All the Gaussians are sorted by depth before the alpha blending calculation.

Static Modeling of the Canonical Hair. To obtain the canonical human hair $\mathcal{G}_c = \{x_c^i, r_c^i, s_c^i, o_c^i, sh_c^i\}_{i=1:N}$, we optimize a 3DGS from multi-view images of one training frame. Note that we initialize the point cloud by sampling on- and off-surface points according to the scalp region of the tracked FLAME mesh and only use image pixels under the hair mask regions for photometric training.

Rigid Hair Transformation between Two Frames. To handle head movement between different frames, we compute per-frame rigid transformations $\{R_i, t_i\}_{i=1:N_f}$ relative to the FLAME mesh in the canonical frame using the ICP algorithm [3]:

$$(R_i, t_i) = \text{ICP}(\mathcal{V}^{scalp}(\beta_i, \psi_i, \phi_i), \mathcal{V}^{scalp}(\beta_c, \psi_c, \phi_c)), \quad (5)$$

where N_f represents the number of all training frames, β_c, ψ_c , and ϕ_c the FLAME parameters of the canonical frame, \mathcal{V}^{scalp} the pre-defined scalp vertices. $\text{ICP}(\cdot)$ computes an alignment (i.e., a rigid transformation) between two shapes (i.e., two point sets) that minimizes the Euclidean distance of the transformed shapes.

With the rigid transformations, we obtain initial hair renderings from the transformed Gaussians $\mathcal{G}_r = \{x_r^i, r_r^i, s_r^i, o_r^i, sh_r^i\}_{i=1:N}$ that are used for later dynamic hair modeling.

Non-Rigid Hair Deformation between Two Frames. To further handle the variations caused by different poses/expressions and obtain sharper renderings, we learn a non-rigid deformation field parameterized by an MLP \mathcal{M}_d :

$$\mathcal{M}_d : \psi \rightarrow (\delta x, \delta r, \delta s, \delta o, \delta c), \quad (6)$$

where ψ describes the FLAME expression parameters. The final Gaussian hair including both rigid and non-rigid deformations is $\mathcal{G}_d = \{x_r^i + \delta x^i, r_r^i + \delta r^i, s_c^i + \delta s^i, o_c^i + \delta o^i, sh_c^i + \delta sh^i\}_{i=1:N}$.

3.3 Occlusion-Aware Blending

Due to the existence of a head mesh, which is a fully opaque object, the correct rendering of this hybrid representation requires only rendering the Gaussians in front of the mesh from the viewing direction and excluding the contributions from the occluded Gaussians.

In our implementation (Fig. 2), we first test the visibility of the Gaussian hair using a “near-z” depth map D_{nz} , which is defined as the depth value of the first Gaussian (depth sorted) whose opacity value is larger than a predefined threshold (0.05 in our experiments). If a pixel’s “near-z” depth is larger than its mesh depth, we know the Gaussians are occluded by the head mesh and do not contribute to this pixel. We denote this binary occlusion mask as $M_o = D_{nz} < D_h$.

For regions under M_o , we know there exist Gaussians in front of the mesh, but we still need to exclude the contributions from the Gaussian occluded by the mesh. For example, when viewed from the front of the head, a ray first intersects the hair in front of the head, then the head, then the hair at the back of the head. We only need to account for the contribution from the Gaussians in front of the head. Thus, we introduce an early-stopping strategy when rendering the Gaussian hair. Specifically, we will stop the color accumulation if the next Gaussian (depth sorted) is too far from the current one for a given ray.

Blending the face image and hair image. Incorporating the aforementioned early-stopping strategy into the alpha accumulating process, we obtain an opacity map A_g for the Gaussian hair. The final blending map for the hair image is $\hat{A}_{hair} = A_g \cdot M_o$. Consequently, the final rendering image \hat{I} of the proposed hybrid representation is obtained by:

$$\hat{I} = \hat{A}_{hair} \cdot \hat{I}_{hair} + (1 - \hat{A}_{hair}) \cdot \hat{I}_{head}, \quad (7)$$

4 Optimizing the Hybrid Mesh-Gaussian Head Avatar

It is highly under-constrained and thus unstable to directly optimize the complete hybrid facial mesh and Gaussian hair avatar from scratch. Therefore, our optimization process of MeGA is divided into three stages in total, including facial mesh optimization, canonical hair optimization, and joint optimization.

Learnable parameters. For convenience, we list all learnable parameters here. For the Gaussian hair, θ_{gs} refers to all learnable parameters of the canonical Gaussian hair. θ_{def} describes the parameters of MLPs used to learn the hair deformation field. For the mesh-based neural head, \hat{T}_{di} is a learnable latent map (i.e., neural texture [30]) expected to represent the diffuse color, θ_v refers to the network parameters of view texture decoder \mathcal{D}_v , from which a view-dependent neural texture map is produced. θ_{dy} refers to the network parameters of the dynamic texture decoder, from which an expression-dependent dynamic neural texture map is produced. θ_{disp} refers to the network parameters of the geometry decoder \mathcal{D}_d , from which a UV displacement map is produced to refine the tracked FLAME mesh. θ_{pix} refers to parameters of the pixel decoder \mathcal{D}_{pix} that decode neural textures into colors.

Optimizing Facial Mesh. In the first stage, we optimize all learnable parameters related to our facial mesh (i.e., θ_{di} , θ_v , θ_{dy} , θ_{disp} , and θ_{pix}) with two per-pixel photometric losses \mathcal{L}_{pho}^F and \mathcal{L}_{di-pho}^F , a D-SSIM loss \mathcal{L}_{ssim}^F , a shrink loss \mathcal{L}_{shr}^F , two depth-based losses \mathcal{L}_d^F and \mathcal{L}_n^F , and three regularization losses \mathcal{L}_{lap}^F , \mathcal{L}_{nc}^F , and \mathcal{L}_{el}^F .

Photometric losses. Specifically, \mathcal{L}_{pho}^F and \mathcal{L}_{ssim}^F provide supervisions for rendered facial colors as:

$$\mathcal{L}_{pho}^F = \|\mathbf{I}_{head} - \hat{\mathbf{I}}_{head}\|_2, \quad \mathcal{L}_{ssim}^F = 1 - \text{SSIM}(\mathbf{I}_{head}, \hat{\mathbf{I}}_{head}), \quad (8)$$

where \mathbf{I}_{head} is the ground truth image of the head part.

We apply an extra L2-based photometric loss $\mathcal{L}_{di-pho}^F = \|\mathbf{I}_{head} - \hat{\mathbf{I}}_{head}^{di}\|_2$ to encourage more meaningful texture decomposition, where $\hat{\mathbf{I}}_{head}^{di}$ is decoded using only the diffuse latent textures \hat{T}_{di} .

Geometric losses. We use depth and its derived normal losses to refine the geometry of the tracked facial mesh as follows:

$$\mathcal{L}_d^F = \|(\mathbf{D}_{head} - \hat{\mathbf{D}}_{head}) \odot \mathbf{M}_d\|_1, \quad \mathcal{L}_n^F = \|N(\mathbf{D}_{head}) - N(\hat{\mathbf{D}}_{head}) \odot \mathbf{M}_d\|, \quad (9)$$

where \mathbf{D}_{head} is the ground truth depth map of the head part reconstructed from multi-view images using Metashape software [25]. $\hat{\mathbf{D}}_{head}$ is the depth map rasterized by our facial mesh and $N(\cdot)$ computes the screen space normals. \mathbf{M}_d is used to penalize those pixels whose depth errors are less than a depth threshold δ_D (set to 5mm) due to the existence of noise.

Shrink loss. Since the estimated FLAME head is usually too big and covers the hair, we introduce a shrink regularization loss \mathcal{L}_{shr}^F for the scalp vertices \mathcal{V}_r^{scalp} , which are obtained by projecting hair masks back to the deformed FLAME mesh.

$$\mathcal{L}_{shr}^F = \|\mathcal{V}_r^{scalp}(\beta, \psi, \phi) - \text{Mean}(\mathcal{V}^{scalp}(\beta, \psi, \phi))\|_2, \quad (10)$$

After shrinking the scalp vertices towards the scalp center, the Gaussians can be generated at the correct location without being occluded by the head mesh.

Regularizations. Three regularization losses ensure that a reasonable facial mesh (i.e., no face crossing, reversing, etc.) can be generated. The mesh laplacian loss \mathcal{L}_{lap}^F and normal consistency loss \mathcal{L}_{nc}^F tend to make our facial mesh smoother. The edge length loss \mathcal{L}_{el}^F is used to keep the rigidity of the facial mesh as much as possible.

In summary, the complete training loss of our facial mesh is the weighted sum of these loss terms:

$$\begin{aligned} \mathcal{L}^F = & \lambda_{pho}\mathcal{L}_{pho}^F + 3 \cdot \lambda_{pho}\mathcal{L}_{di-pho}^F + \lambda_d\mathcal{L}_d^F + \lambda_n\mathcal{L}_n^F + \lambda_{ssim}\mathcal{L}_{ssim}^F \\ & + \lambda_{shr}\mathcal{L}_{shr}^F + \mathcal{L}_{reg}^F, \end{aligned} \quad (11)$$

where $\mathcal{L}_{reg}^F = \lambda_{lap}\mathcal{L}_{lap}^F + \lambda_{nc}\mathcal{L}_{nc}^F + \lambda_{el}\mathcal{L}_{el}^F$.

Optimizing Canonical Gaussian Hair. As mentioned in Sec. 3.2, Using points sampled around the tracked FLAME mesh (Sec. 3.2) as initialization, we optimize a canonical Gaussian hair (i.e., θ_{gs}) using two appearance losses \mathcal{L}_{pho}^H and \mathcal{L}_{ssim}^H as in 3DGS [15], a silhouette loss \mathcal{L}_{silh}^H , and a regularization loss \mathcal{L}_{sol}^H .

Specifically, two appearance losses are defined as:

$$\mathcal{L}_{pho}^H = \|\mathbf{I}_{hair} - \hat{\mathbf{I}}_{hair}\|_2, \quad \mathcal{L}_{ssim}^H = 1 - \text{SSIM}(\mathbf{I}_{hair}, \hat{\mathbf{I}}_{hair}), \quad (12)$$

where \mathbf{I}_{hair} is the ground truth image of the hair part.

To encourage a better disentanglement of the facial mesh and Gaussian hair, we introduce a silhouette loss:

$$\mathcal{L}_{silh}^H = \|(\mathbf{M}_{hair} - \hat{\mathbf{A}}_{hair}) \odot \Delta\|_1, \quad \Delta(x_i) = \min_{x_j \in \mathbf{M}_{hair}} (\|x_i - x_j\|_2). \quad (13)$$

where \mathbf{M}_{hair} is the ground truth hair mask, obtained using a standard face parsing algorithm [17]. $\Delta(\cdot)$ is a weight so that distant incorrect pixels on the rendered mask are penalized more than closer pixels.

We introduce a regularization loss that encourages the Gaussian hair to generate a solid hair mask except for its boundary regions. Mathematically, $\mathcal{L}_{sol}^c = \|(\mathbf{1} - \hat{\mathbf{A}}_{hair}) \odot \text{Erode}(\mathbf{M}_{hair})\|_1$, where $\text{Erode}(\cdot)$ is the erosion (shrink) operation.

In summary, the complete loss used to train the canonical hair is defined as:

$$\mathcal{L}^H = \lambda_{pho}\mathcal{L}_{pho}^H + \lambda_{ssim}\mathcal{L}_{ssim}^H + \lambda_{silh}\mathcal{L}_{silh}^H + \lambda_{sol}\mathcal{L}_{sol}^H \quad (14)$$

Joint Optimization. With proper initializations of the neural mesh and canonical Gaussian hair, we jointly optimize the hybrid mesh-Gaussian avatar on all the frames mainly to improve the quality of the face-hair overlapping region using the following objective.

$$\begin{aligned} \mathcal{L} = & \lambda_{pho}\mathcal{L}_{pho} + 3\lambda_{pho}\mathcal{L}_{di-pho}^F + \lambda_{ssim}\mathcal{L}_{ssim}^H + \lambda_{silh}\mathcal{L}_{silh}^H + \lambda_{sol}\mathcal{L}_{sol}^H \\ & + \lambda_n(\|\delta r\|_2 + \|\delta s\|_2 + \|\delta o\|_2 + \|\delta c\|_2) + \lambda_{aiap}\mathcal{L}_{aiap}, \end{aligned} \quad (15)$$

Note that the parameters of mesh deformation MLP θ_{disp} and the canonical Gaussian hair θ_{gs} are fixed. And we need to optimize the previously untrained hair deformation MLP \mathcal{M}_d . New regularizations are introduced to constrain the per-Gaussian update as well as an as-isometric-as-possible loss \mathcal{L}_{aiap} [27] to encourage rigidity of the Gaussian hair.

5 Editing Head Avatars

Due to the disentangled facial mesh and Gaussian hair, our MeGA representation naturally supports some editing operations.

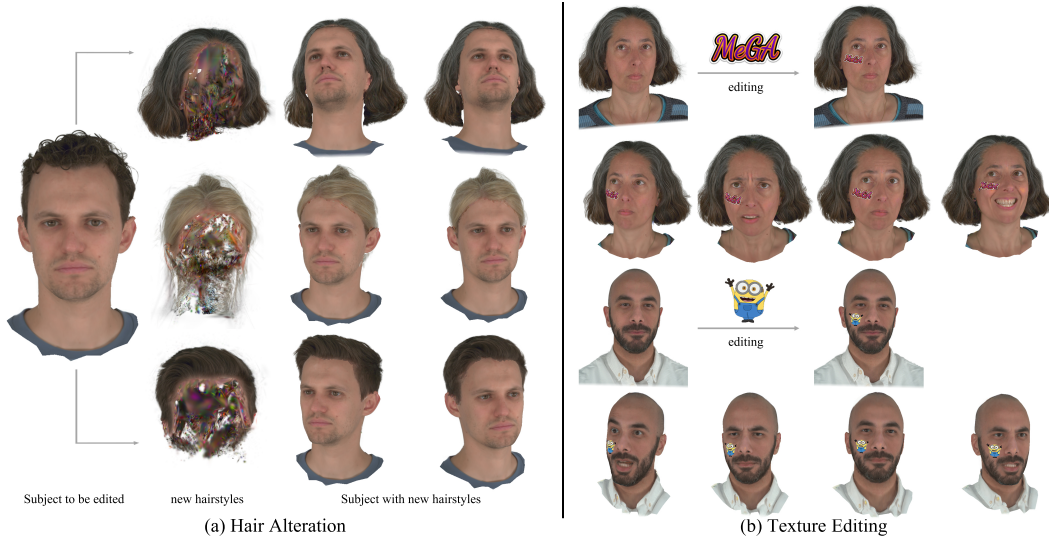


Figure 3: **Hairstyle Alteration and Texture Editing.** MeGA naturally supports hairstyle alteration and texture editing. The edited head avatar can be rendered in different views and expressions.

Table 1: **Comparisons with State-of-the-Art Methods on novel expression synthesis.** MeGA achieves better LPIPS, SSIM, and PSNR (1dB higher than the 2nd best method on average). We bold (underline) the best (2nd best) results.

Subject	MeGA (Ours)			GaussianAvatars			PointAvatars		
	PSNR \uparrow	SSIM \uparrow	LPIPS \downarrow	PSNR \uparrow	SSIM \uparrow	LPIPS \downarrow	PSNR \uparrow	SSIM \uparrow	LPIPS \downarrow
074	29.32	<u>0.917</u>	<u>0.096</u>	28.90	0.919	0.094	24.24	0.883	0.132
104	27.80	<u>0.921</u>	<u>0.098</u>	27.60	0.937	0.094	22.57	0.899	0.111
218	32.76	0.968	0.042	<u>30.89</u>	<u>0.962</u>	<u>0.045</u>	28.25	0.935	0.073
253	36.06	0.968	0.038	<u>33.12</u>	<u>0.964</u>	<u>0.041</u>	26.33	0.925	0.081
264	34.05	0.966	0.044	33.36	0.971	<u>0.046</u>	27.12	0.939	0.076
302	33.50	0.954	0.050	32.28	<u>0.945</u>	<u>0.062</u>	25.88	0.916	0.156
304	29.02	0.891	0.082	29.43	0.903	0.081	23.98	0.874	0.121
306	33.16	0.962	<u>0.045</u>	32.57	<u>0.948</u>	0.044	25.54	0.922	0.079
460	36.56	0.975	0.027	34.94	<u>0.974</u>	<u>0.031</u>	28.24	0.952	0.099
avg.	32.47	0.947	0.058	<u>31.45</u>	0.947	<u>0.060</u>	25.79	0.916	0.103

Hairstyle Alteration. As shown in Fig. 1, our approach can easily update A’s hairstyle with B’s after alignment (with scaling). Specifically, we load subject A’s facial mesh (i.e., θ_{di} , θ_v , θ_{dy} , θ_{disp} , and θ_{pix}) and load subject B’s Gaussian hair (i.e., θ_{gs} and θ_{def}). Then, an ICP-based alignment (with scaling) is conducted to align B’s hair to A’s.

Facial Texture Editing. Our MeGA can easily support texture editing by updating the diffuse neural texture map \hat{T}_{di} according to the painted image I_p and its corresponding mask M_p similar to NeuMesh [39]. Specifically, to edit facial textures, we first remap the 2d painting mask to the UV space, obtaining a mask M_p^{uv} . Only the latent codes under this mask will be optimized in the subsequent optimization. Then we optimize these codes in the diffuse texture map \hat{T}_{di} with a learning rate 0.01 and the pixel decoder θ_{pix} with a learning rate 0.0001. Slightly finetuning the pixel decoder allows it to show new colors that are not seen during modeling head avatars.

Note that we calculate losses for the complete image on the view I_p and calculate losses outside the painting mask on other views. Optimizing the losses on the other views serves as a regularization of the pixel decoder \mathcal{D}_{pix} , resulting in minimal changes on the non-painting regions.

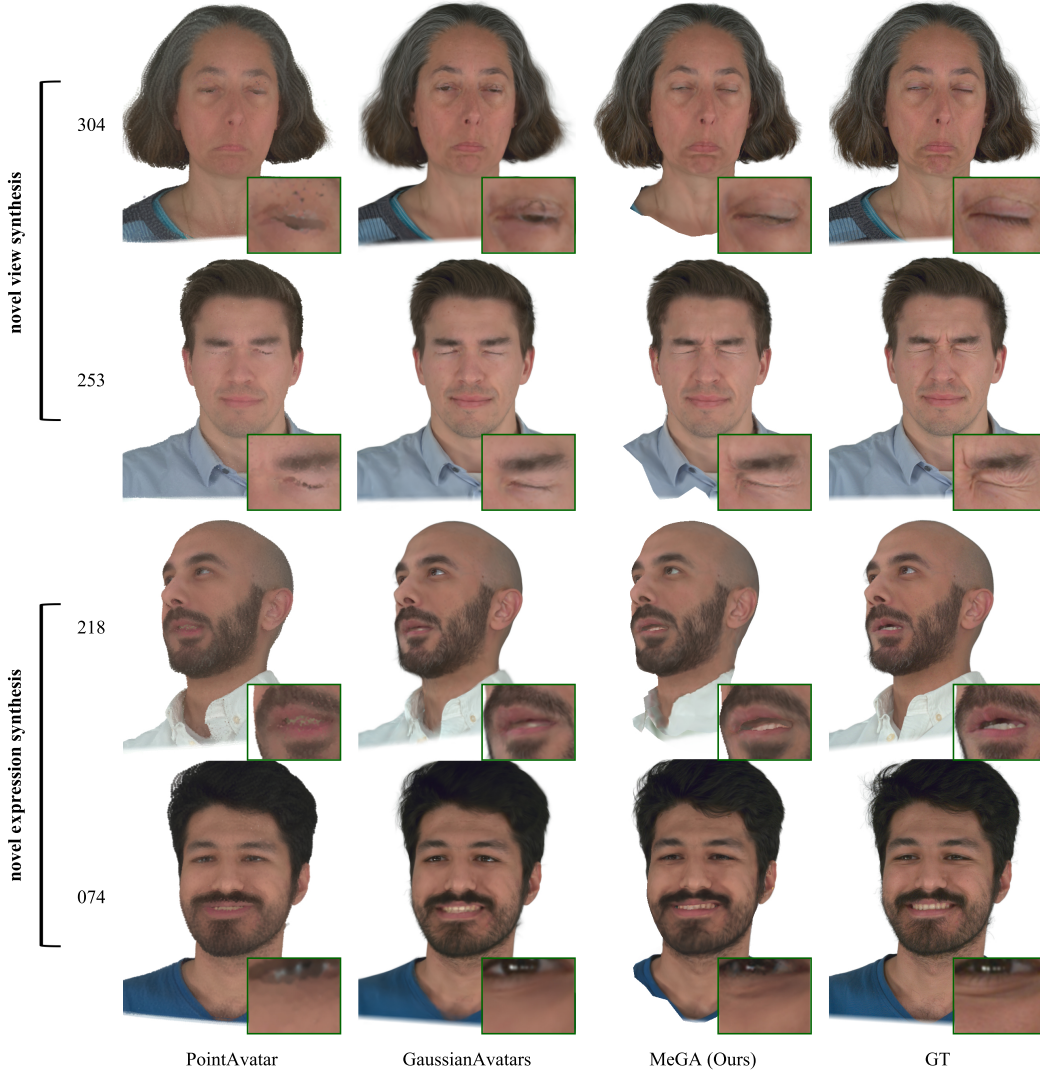


Figure 4: **Qualitative Comparisons with State-of-the-Art Methods.** MeGA generates more realistic facial renditions compared to previous state-of-the-art methods, especially in terms of expression matching and detailed skin textures (e.g., wrinkles).

6 Experiments

We evaluate our approach on the NeRSemble dataset [16], which includes multi-view videos of each subject and calibrated camera parameters of all 16 cameras. GaussianAvatars [26] downsample the images to a resolution of 802×550 and generate the foreground mask for each image. Based on their processed images, we further obtain facial parsing results for each image using an open-source algorithm [17] and a depth map for each frame using Metashape software [25].

We train our approach with the same train/test splits as GaussianAvatars [26]. Specifically, 9 out of 10 expression sequences and 15 out of 16 available cameras are used for training, and the remaining camera and expression sequences are used for evaluation. All the metrics are calculated based on image pixels under the rasterization mask.

6.1 Comparisons with State-of-the-Art Methods

We conduct a comparison with PointAvatars [42] and GaussianAvatars [26] to show the superiority of our approach in terms of novel view synthesis (“NVS”, i.e., render the training expressions for the held-out view) and novel expression synthesis (“NES”, i.e., render the unseen expressions during

Table 2: **Ablation Studies on Subject 306.** We demonstrate the effectiveness of each proposed component in MeGA. (a) shows the importance of our view-dependent texture \hat{T}_v and expression-dependent texture \hat{T}_{dy} in generating high-quality renderings. (b) shows that the UV displacement map \hat{G}_d improves geometric details and produce better results. (c) shows the superiority of our occlusion-aware blending module. (d) demonstrates that any regularization presents positive effects on performance.

Label	Name	Texture	Disp. Map (\hat{G}_d)	Blending	Losses	PSNR \uparrow	SSIM \uparrow	LPIPS \downarrow
	MeGA (Ours)		✓			33.16	0.962	0.045
(a.1)	MeGA-noview	w/o \hat{T}_v	✓			31.68	0.958	0.053
(a.2)	MeGA-nodyn	w/o \hat{T}_{dy}	✓			32.81	0.959	0.050
(b)	MeGA-nodisp		✗			32.99	0.959	0.054
(c.1)	MeGA-gsdepth		✓	using alpha-acc. depths		27.94	0.950	0.068
(c.2)	MeGA-3dprune		✓	prune Gaussians in 3d		26.60	0.939	0.077
(d.1)	MeGA-nodipho		✓		w/o \mathcal{L}_{di-pho}^h	33.10	0.961	0.046
(d.2)	MeGA-noaiap		✓		w/o \mathcal{L}_{aiap}	33.06	0.961	0.048
(d.3)	MeGA-noheadreg		✓		w/o \mathcal{L}_{reg}^h	32.51	0.959	0.051

training for all 16 views). All baselines are trained from scratch using their public codes. Due to the limited memory of NVIDIA V100 GPUs (32GB), we set the maximum number of points in PointAvatar to 240,000. Tab. 1 shows results on NES. Our approach obtains the best PSNR, SSIM, and LPIPS averaged among all 9 subjects. Fig. 4 demonstrates that our approach produces higher-fidelity facial renditions, especially when modeling the detailed skin appearance (e.g., wrinkles). MeGA can model such geometric details due to the use of expression-dependent dynamic textures (i.e., \hat{T}_{dy}). In contrast, GaussianAvatars requires highly accurate semantic correspondences between frames to model such geometry details due to the lack of expression-dependent colors. More results (including quantitative results of NVS and cross-identity reenactment) are shown in our Supp. Mat.

6.2 Experiments on Head Editing

We only show our results for qualitative evaluation since no previous methods¹, to the best of our knowledge, is suitable for the following head editing types (i.e., hairstyle alteration, and texture editing).

MeGA supports changing someone’s hairstyle to a new one (i.e., short, medium, and long hair) from another MeGA-pretrained model (Fig. 3a). Recomposed head avatars can be rendered in novel views and novel expressions. Fig. 3b demonstrates the texture editing functionality. Given a painted image of the subject and the corresponding painting mask, MeGA can embed this modification into the 3D head avatar to render view-consistent images in novel views and expressions.

6.3 Ablation Studies

In this section, we present a series of ablation studies to verify the effectiveness of our major design choices.

Disentangled Texture Maps. Tab. 2 (a.1) and (a.2) demonstrate the roles of our two disentangled texture maps, and the visual results are shown in Fig. 5. When the view texture \hat{T}_v is disabled (i.e., MeGA-noview), MeGA struggles to handle view-dependent effects and shows an even brightness across the face, especially inside the mouth (unnatural shadows). The quantitative metrics also get worse (33.16 vs. 31.68 PSNR). When the expression-dependent dynamic texture \hat{T}_{dy} is disabled (i.e., MeGA-nodyn), MeGA no longer captures detailed skin appearance (e.g., wrinkles), although the quantitative results are similar (33.16 vs. 32.81 PSNR).

Geometry Refinement. We investigate the effect of using a UV displacement map \hat{G}_d for geometry detail improvement. The quantitative result is reported in Tab. 2 (b). Using a UV displacement map

¹Previous mesh-based methods [23, 9] are not suitable for texture editing due to the entanglement of base colors and view-dependent effects.

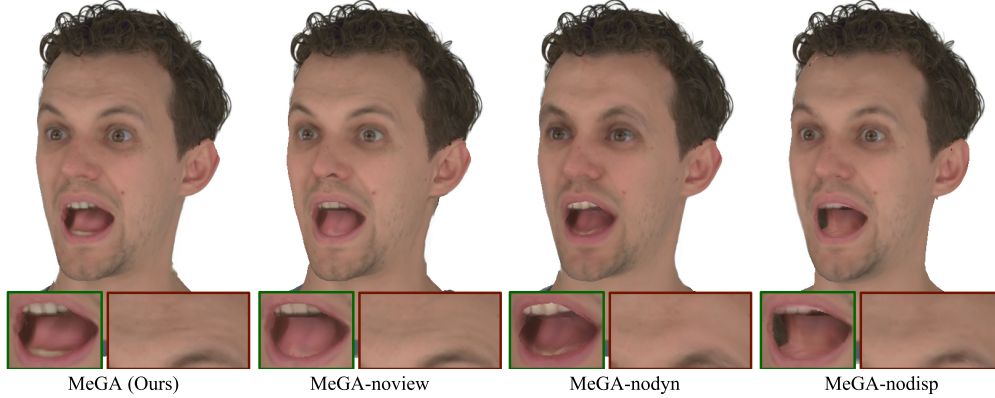


Figure 5: **Effects of disentangled texture maps and the UV displacement map.** Disabling any of the texture maps results in a worse appearance in the facial region (i.e., MeGA-noview and MeGA-nodyn). No UV displacement map leads to a lack of geometric details and produces unrealistic renderings.

\hat{G}_d improves the evaluation metrics (33.16 vs 32.99 PSNR, 0.054 vs 0.045 LPIPS) and leads to better visual results (Fig. 5).

Different Blending Strategies. To verify the effectiveness of our mesh occlusion-aware blending approach, we test other potential blending strategies and report quantitative results in Tab. 2(c.1)-(c.2). “MeGA-gsdepth” attempts to obtain the visibility of the Gaussian hair using the 3DGS-rendered depth map, instead of the “near-z” depth map. Since the 3DGS-rendered depth map is not smooth and exists many noises, “MeGA-gsdepth” struggles to obtain correct occlusion between the mesh and the Gaussians during training, causing the optimization not convergent². “MeGA-3dprune” prunes the Gaussians behind the facial mesh before rendering the hair image for a view, and then the hair and head images can be naturally blended using the opacity map rendered by 3DGS. However, using such a “hard” pruning operation severely affects the optimization stability³, resulting in abruptly decreased results (33.16 vs. 26.60 PSNR).

Regularizations. Tab. 2(d.1)-(d.3) shows the results after removing some regularizations. The removal of each regularization will degrade the performance. Note that removing $\mathcal{L}_{di,pho}^h$, although seems harmless on the metrics, will entangle the view- and expression-dependent effects into the diffuse texture map \hat{T}_{di} and harms the following texture editing, which is verified in our Supp. Mat.

7 Conclusion

In this paper, we present hybrid mesh-Gaussian head avatars (MeGA), which employ neural mesh for face modeling and 3DGS for hair modeling. For high-quality facial modeling, we enhance the FLAME mesh and decode a UV displacement map for geometric details. Facial colors are decoded from a neural texture map that consists of disentangled diffuse texture \hat{T}_{di} , view-dependent texture \hat{T}_v , and dynamic texture \hat{T}_{dy} . For high-quality hair models, we build a static 3DGS hair and employ a rigid transformation combined with an MLP-based deformation field for animation. The final renderings are obtained by blending the hair and head parts with our occlusion-aware blending module. Moreover, MeGA naturally supports various editing functionalities, including hairstyle alteration and texture editing.

²The optimization objective of 3DGS is constantly changing due to unstable occlusion relations between the mesh and 3DGS.

³Small update on a Gaussian’s location results in obvious appearance change if the point is close to the mesh.

References

- [1] Bai, Z., Tan, F., Huang, Z., Sarkar, K., Tang, D., Qiu, D., Meka, A., Du, R., Dou, M., Orts-Escolano, S., Pandey, R., Tan, P., Beeler, T., Fanello, S., Zhang, Y.: Learning personalized high quality volumetric head avatars from monocular RGB videos. In: IEEE/CVF Conference on Computer Vision and Pattern Recognition, CVPR 2023, Vancouver, BC, Canada, June 17-24, 2023. pp. 16890–16900. IEEE (2023). <https://doi.org/10.1109/CVPR52729.2023.01620>, <https://doi.org/10.1109/CVPR52729.2023.01620>
- [2] Bao, L., Lin, X., Chen, Y., Zhang, H., Wang, S., Zhe, X., Kang, D., Huang, H., Jiang, X., Wang, J., et al.: High-fidelity 3d digital human head creation from rgb-d selfies. *ACM TOG* **41**(1), 1–21 (2021)
- [3] Besl, P.J., McKay, N.D.: A method for registration of 3-d shapes. *IEEE Trans. Pattern Anal. Mach. Intell.* **14**(2), 239–256 (1992). <https://doi.org/10.1109/34.121791>, <https://doi.org/10.1109/34.121791>
- [4] Blanz, V., Vetter, T.: A morphable model for the synthesis of 3d faces. In: Waggenspack, W.N. (ed.) *Proceedings of the 26th Annual Conference on Computer Graphics and Interactive Techniques, SIGGRAPH 1999*, Los Angeles, CA, USA, August 8-13, 1999. pp. 187–194. ACM (1999)
- [5] Chen, Y., Wang, L., Li, Q., Xiao, H., Zhang, S., Yao, H., Liu, Y.: Monogaussianavatar: Monocular gaussian point-based head avatar. *CoRR* **abs/2312.04558** (2023). <https://doi.org/10.48550/ARXIV.2312.04558>, <https://doi.org/10.48550/arXiv.2312.04558>
- [6] Dhano, H., Nie, Y., Moreau, A., Song, J., Shaw, R., Zhou, Y., Pérez-Pellitero, E.: Headgas: Real-time animatable head avatars via 3d gaussian splatting. *CoRR* **abs/2312.02902** (2023). <https://doi.org/10.48550/ARXIV.2312.02902>, <https://doi.org/10.48550/arXiv.2312.02902>
- [7] Gafni, G., Thies, J., Zollhofer, M., Nießner, M.: Dynamic neural radiance fields for monocular 4d facial avatar reconstruction. In: *CVPR*. pp. 8649–8658 (2021)
- [8] Gao, X., Zhong, C., Xiang, J., Hong, Y., Guo, Y., Zhang, J.: Reconstructing personalized semantic facial nerf models from monocular video. *ACM TOG* **41**(6), 1–12 (2022)
- [9] Grassal, P., Prinzler, M., Leistner, T., Rother, C., Nießner, M., Thies, J.: Neural head avatars from monocular RGB videos. In: *IEEE/CVF Conference on Computer Vision and Pattern Recognition, CVPR 2022*, New Orleans, LA, USA, June 18-24, 2022. pp. 18632–18643. IEEE (2022). <https://doi.org/10.1109/CVPR52688.2022.01810>, <https://doi.org/10.1109/CVPR52688.2022.01810>
- [10] He, Z., Du, R., Perlin, K.: Collabovr: A reconfigurable framework for creative collaboration in virtual reality. In: *2020 IEEE International Symposium on Mixed and Augmented Reality, ISMAR 2020*, Recife/Porto de Galinhas, Brazil, November 9-13, 2020. pp. 542–554. IEEE, Brazil (2020). <https://doi.org/10.1109/ISMAR50242.2020.00082>, <https://doi.org/10.1109/ISMAR50242.2020.00082>
- [11] Hong, Y., Peng, B., Xiao, H., Liu, L., Zhang, J.: Headnerf: A real-time nerf-based parametric head model. In: *CVPR*. pp. 20374–20384 (2022)
- [12] Hong, Y., Peng, B., Xiao, H., Liu, L., Zhang, J.: Headnerf: A realtime nerf-based parametric head model. In: *IEEE/CVF Conference on Computer Vision and Pattern Recognition, CVPR 2022*, New Orleans, LA, USA, June 18-24, 2022. pp. 20342–20352. IEEE (2022). <https://doi.org/10.1109/CVPR52688.2022.01973>, <https://doi.org/10.1109/CVPR52688.2022.01973>
- [13] Hu, L., Saito, S., Wei, L., Nagano, K., Seo, J., Fursund, J., Sadeghi, I., Sun, C., Chen, Y.C., Li, H.: Avatar digitization from a single image for real-time rendering. *ACM TOG* **36**(6), 1–14 (2017)
- [14] Ichim, A.E., Bouaziz, S., Pauly, M.: Dynamic 3d avatar creation from hand-held video input. *ACM TOG* **34**(4), 1–14 (2015)
- [15] Kerbl, B., Kopanas, G., Leimkühler, T., Drettakis, G.: 3d gaussian splatting for real-time radiance field rendering. *ACM Trans. Graph.* **42**(4), 139:1–139:14 (2023). <https://doi.org/10.1145/3592433>, <https://doi.org/10.1145/3592433>

- [16] Kirschstein, T., Qian, S., Giebenhain, S., Walter, T., Nießner, M.: Nersemble: Multi-view radiance field reconstruction of human heads. *ACM TOG* **42**(4), 161:1–161:14 (2023). <https://doi.org/10.1145/3592455>, <https://doi.org/10.1145/3592455>
- [17] Lee, C.H., Liu, Z., Wu, L., Luo, P.: Maskgan: Towards diverse and interactive facial image manipulation. In: *IEEE Conference on Computer Vision and Pattern Recognition (CVPR)* (2020)
- [18] Li, T., Bolkart, T., Black, M.J., Li, H., Romero, J.: Learning a model of facial shape and expression from 4d scans. *ACM Trans. Graph.* **36**(6), 194:1–194:17 (2017). <https://doi.org/10.1145/3130800.3130813>, <https://doi.org/10.1145/3130800.3130813>
- [19] Lombardi, S., Saragih, J.M., Simon, T., Sheikh, Y.: Deep appearance models for face rendering. *ACM Trans. Graph.* **37**(4), 68 (2018). <https://doi.org/10.1145/3197517.3201401>, <https://doi.org/10.1145/3197517.3201401>
- [20] Lombardi, S., Simon, T., Saragih, J., Schwartz, G., Lehrmann, A., Sheikh, Y.: Neural volumes: learning dynamic renderable volumes from images. *ACM TOG* **38**(4), 1–14 (2019)
- [21] Lombardi, S., Simon, T., Schwartz, G., Zollhoefer, M., Sheikh, Y., Saragih, J.: Mixture of volumetric primitives for efficient neural rendering. *ACM TOG* **40**(4), 1–13 (2021)
- [22] Lombardi, S., Simon, T., Schwartz, G., Zollhöfer, M., Sheikh, Y., Saragih, J.M.: Mixture of volumetric primitives for efficient neural rendering. *ACM Trans. Graph.* **40**(4), 59:1–59:13 (2021). <https://doi.org/10.1145/3450626.3459863>, <https://doi.org/10.1145/3450626.3459863>
- [23] Ma, S., Simon, T., Saragih, J.M., Wang, D., Li, Y., la Torre, F.D., Sheikh, Y.: Pixel codec avatars. In: *IEEE Conference on Computer Vision and Pattern Recognition, CVPR 2021, virtual, June 19-25, 2021*. pp. 64–73. *Computer Vision Foundation / IEEE* (2021). <https://doi.org/10.1109/CVPR46437.2021.00013>, https://openaccess.thecvf.com/content/CVPR2021/html/Ma_Pixel_Codec_Avatars_CVPR_2021_paper.html
- [24] Orts-Escolano, S., Rhemann, C., Fanello, S.R., Chang, W., Kowdle, A., Degtyarev, Y., Kim, D., Davidson, P.L., Khamis, S., Dou, M., Tankovich, V., Loop, C.T., Cai, Q., Chou, P.A., Mennicken, S., Valentin, J.P.C., Pradeep, V., Wang, S., Kang, S.B., Kohli, P., Lutchyn, Y., Keskin, C., Izadi, S.: Holoportation: Virtual 3d teleportation in real-time. In: *Rekimoto, J., Igarashi, T., Wobbrock, J.O., Avrahami, D. (eds.) Proceedings of the 29th Annual Symposium on User Interface Software and Technology, UIST 2016, Tokyo, Japan, October 16-19, 2016*. pp. 741–754. *ACM*, . (2016)
- [25] Over, J.S.R., Ritchie, A.C., Kranenburg, C.J., Brown, J.A., Buscombe, D.D., Noble, T., Sherwood, C.R., Warrick, J.A., Wernette, P.A.: *Processing coastal imagery with agisoft metashape professional edition, version 1.6—structure from motion workflow documentation*. Tech. rep., *US Geological Survey* (2021)
- [26] Qian, S., Kirschstein, T., Schoneveld, L., Davoli, D., Giebenhain, S., Nießner, M.: Gaussianavatars: Photorealistic head avatars with rigged 3d gaussians. *CoRR* **abs/2312.02069** (2023). <https://doi.org/10.48550/ARXIV.2312.02069>, <https://doi.org/10.48550/arXiv.2312.02069>
- [27] Qian, Z., Wang, S., Mihajlovic, M., Geiger, A., Tang, S.: 3dgs-avatar: Animatable avatars via deformable 3d gaussian splatting. *CoRR* **abs/2312.09228** (2023). <https://doi.org/10.48550/ARXIV.2312.09228>, <https://doi.org/10.48550/arXiv.2312.09228>
- [28] Schönberger, J.L., Frahm, J.: Structure-from-motion revisited. In: *2016 IEEE Conference on Computer Vision and Pattern Recognition, CVPR 2016, Las Vegas, NV, USA, June 27-30, 2016*. pp. 4104–4113. *IEEE Computer Society* (2016). <https://doi.org/10.1109/CVPR.2016.445>, <https://doi.org/10.1109/CVPR.2016.445>
- [29] Sevastopolsky, A., Grassal, P., Giebenhain, S., Athar, S., Verdoliva, L., Nießner, M.: Headcraft: Modeling high-detail shape variations for animated 3dmmms. *CoRR* **abs/2312.14140** (2023). <https://doi.org/10.48550/ARXIV.2312.14140>, <https://doi.org/10.48550/arXiv.2312.14140>
- [30] Thies, J., Zollhöfer, M., Nießner, M.: Deferred neural rendering: image synthesis using neural textures. *ACM Trans. Graph.* **38**(4), 66:1–66:12 (2019). <https://doi.org/10.1145/3306346.3323035>, <https://doi.org/10.1145/3306346.3323035>

- [31] Waggoner, Z.: My avatar, my self: Identity in video role-playing games. McFarland, . (2009)
- [32] Wang, C., Kang, D., Cao, Y., Bao, L., Shan, Y., Zhang, S.: Neural point-based volumetric avatar: Surface-guided neural points for efficient and photorealistic volumetric head avatar. In: Kim, J., Lin, M.C., Bickel, B. (eds.) SIGGRAPH Asia 2023 Conference Papers, SA 2023, Sydney, NSW, Australia, December 12-15, 2023. pp. 50:1–50:12. ACM (2023). <https://doi.org/10.1145/3610548.3618204>, <https://doi.org/10.1145/3610548.3618204>
- [33] Wang, J., Xie, J.C., Li, X., Xu, F., Pun, C.M., Gao, H.: Gaussianhead: High-fidelity head avatars with learnable gaussian derivation (2024)
- [34] Wang, P., Bai, X., Billingham, M., Zhang, S., Zhang, X., Wang, S., He, W., Yan, Y., Ji, H.: AR/MR remote collaboration on physical tasks: A review. *Robotics Comput. Integr. Manuf.* **72**, 102071 (2021)
- [35] Wang, Z., Bagautdinov, T., Lombardi, S., Simon, T., Saragih, J., Hodgins, J., Zollhofer, M.: Learning compositional radiance fields of dynamic human heads. In: CVPR. pp. 5704–5713 (2021)
- [36] Xu, Y., Chen, B., Li, Z., Zhang, H., Wang, L., Zheng, Z., Liu, Y.: Gaussian head avatar: Ultra high-fidelity head avatar via dynamic gaussians. *CoRR* **abs/2312.03029** (2023). <https://doi.org/10.48550/ARXIV.2312.03029>, <https://doi.org/10.48550/arXiv.2312.03029>
- [37] Xu, Y., Wang, L., Zhao, X., Zhang, H., Liu, Y.: Avatarmav: Fast 3d head avatar reconstruction using motion-aware neural voxels. In: Brunvand, E., Sheffer, A., Wimmer, M. (eds.) ACM SIGGRAPH 2023 Conference Proceedings, SIGGRAPH 2023, Los Angeles, CA, USA, August 6-10, 2023. pp. 47:1–47:10. ACM (2023). <https://doi.org/10.1145/3588432.3591567>, <https://doi.org/10.1145/3588432.3591567>
- [38] Xu, Y., Wang, L., Zhao, X., Zhang, H., Liu, Y.: Avatarmav: Fast 3d head avatar reconstruction using motion-aware neural voxels. In: ACM SIGGRAPH 2023 Conference Proceedings. pp. 1–10 (2023)
- [39] Yang, B., Bao, C., Zeng, J., Bao, H., Zhang, Y., Cui, Z., Zhang, G.: Neumesh: Learning disentangled neural mesh-based implicit field for geometry and texture editing. In: Avidan, S., Brostow, G.J., Cissé, M., Farinella, G.M., Hassner, T. (eds.) Computer Vision - ECCV 2022 - 17th European Conference, Tel Aviv, Israel, October 23-27, 2022, Proceedings, Part XVI. Lecture Notes in Computer Science, vol. 13676, pp. 597–614. Springer (2022). https://doi.org/10.1007/978-3-031-19787-1_34, https://doi.org/10.1007/978-3-031-19787-1_34
- [40] Zhao, X., Wang, L., Sun, J., Zhang, H., Suo, J., Liu, Y.: Havatar: High-fidelity head avatar via facial model conditioned neural radiance field. *ACM TOG* **43**(1), 1–16 (2023)
- [41] Zheng, Y., Abrevaya, V.F., Bühler, M.C., Chen, X., Black, M.J., Hilliges, O.: Im avatar: Implicit morphable head avatars from videos. In: CVPR. pp. 13545–13555 (2022)
- [42] Zheng, Y., Yifan, W., Wetzstein, G., Black, M.J., Hilliges, O.: Pointavatar: Deformable point-based head avatars from videos. In: IEEE/CVF Conference on Computer Vision and Pattern Recognition, CVPR 2023, Vancouver, BC, Canada, June 17-24, 2023. pp. 21057–21067. IEEE (2023). <https://doi.org/10.1109/CVPR52729.2023.02017>, <https://doi.org/10.1109/CVPR52729.2023.02017>
- [43] Zhou, M., Hyder, R., Xuan, Z., Qi, G.: Ultravatar: A realistic animatable 3d avatar diffusion model with authenticity guided textures. *CoRR* **abs/2401.11078** (2024). <https://doi.org/10.48550/ARXIV.2401.11078>, <https://doi.org/10.48550/arXiv.2401.11078>
- [44] Zielonka, W., Bolkart, T., Thies, J.: Instant volumetric head avatars. In: CVPR. pp. 4574–4584 (2023)